CNGA3 Deficiency Affects Cone Synaptic Terminal Structure and Function and Leads to Secondary Rod Dysfunction and Degeneration

Jianhua Xu,[1] *Lynsie M. Morris,*[1] *Stylianos Michalakis,*[2] *Martin Biel,*[2] *Steven J. Fliesler,*[3,4,5,6] *David M. Sherry,*[1,7,8] *and Xi-Qin Ding*[1]

Purpose. To investigate rod function and survival after cone dysfunction and degeneration in a mouse model of cone cyclic nucleotide-gated (CNG) channel deficiency.

Methods. Rod function and survival in mice with cone CNG channel subunit CNGA3 deficiency (CNGA3$^{-/-}$ mice) were evaluated by electroretinographic (ERG), morphometric, and Western blot analyses. The arrangement, integrity, and ultrastructure of photoreceptor terminals were investigated by immunohistochemistry and electron microscopy.

Results. The authors found loss of cone function and cone death accompanied by impairment of rods and rod-driven signaling in CNGA3$^{-/-}$ mice. Scotopic ERG b-wave amplitudes were reduced by 15% at 1 month, 30% at 6 months, and 40% at 9 months and older, while scotopic a-wave amplitudes were decreased by 20% at 9 months, compared with ERGs of age-matched wild-type mice. Outer nuclear layer thickness in CNGA3$^{-/-}$ retina was reduced by 15% at 12 months compared with age-matched wild-type controls. This was accompanied by a 30%–40% reduction in expression of rod-specific proteins, including rhodopsin, rod transducin α-subunit, and glutamic acid-rich protein (GARP). Cone terminals in the CNGA3$^{-/-}$ retina showed a progressive loss of neurochemical and ultrastructural integrity. Abnormalities were observed as early as 1 month. Disorganized rod terminal ultrastructure was noted by 12 months.

Conclusions. These findings demonstrate secondary rod impairment and degeneration after cone degeneration in mice with cone CNG channel deficiency. Loss of cone phototransduction accompanies the compromised integrity of cone terminals. With time, rod synaptic structure, function, and viability also become compromised. (*Invest Ophthalmol Vis Sci.* 2012;53:1117–1129) DOI:10.1167/iovs.11-8168

Rod and cone photoreceptors degenerate under a variety of pathologic conditions, including those caused by bright light exposure and a wide array of hereditary retinal diseases, such as retinitis pigmentosa (RP), macular degeneration (MD), and cone-rod dystrophies. Defects in a large number of genes are linked to inherited retinal degenerative disorders (see more information at http://www.sph.uth.tmc.edu/RetNet/disease.htm). These genes include those encoding phototransduction-related proteins, such as rhodopsin, subunits of cyclic nucleotide phosphodiesterase (PDE), and cyclic nucleotide-gated (CNG) channel subunits, as well as genes encoding photoreceptor outer segment structural proteins, such as peripherin/*rds*.

Secondary, or nonautonomous photoreceptor degeneration occurs when a disease gene expressed specifically in one type of photoreceptor (e.g., rods) leads to loss of photoreceptors that do not express the disease gene. For example, RP arising from defects in the rod-specific PDE gene leads to secondary loss of cones. Death of cones after rod death in RP is a characteristic of secondary photoreceptor degeneration associated with disease progression, and is also found in other human photoreceptor degenerations. Indeed, cone degeneration secondary to rod death has been studied intensively in human RP patients and in animal models of RP.[1–4] In contrast, our understanding of the impact of cone degeneration on rod function and survival is very limited. Though early reports suggested normal or nearly normal rod function in patients with cone degenerations, such as achromatopsia and cone dystrophy,[5–7] several recent studies have reported reduced rod electroretinographic (ERG) responses and disrupted rod photoreceptor mosaic in such disorders,[8–10] suggesting that secondary impairment of rod function and viability may be a common consequence of primary cone degeneration.

CNG channels, which are localized to the plasma membrane of the outer segment of rods and cones, play a pivotal role in phototransduction. In darkness, rod CNG channels are activated by binding of cyclic guanosine monophosphate (cGMP), allowing a steady inward cation (Na^+ and Ca^{2+}) current. Light triggers a sequence of enzymatic reactions that leads to the hydrolysis of cGMP, resulting in CNG channel closure, reduction in the inward cation current, and membrane hyperpolarization.[11–14] A similar transduction scheme exists in cones. However, the CNG channels of rods and cones are formed from different A and B subunits, leading to profound differences in cGMP sensitivity, Ca^{2+} permeation, and functional modulation.[15,16] The rod CNG channel is formed from

From the Departments of [1]Cell Biology and [8]Pharmaceutical Sciences, and [7]Oklahoma Center for Neurosciences, The University of Oklahoma Health Sciences Center, Oklahoma City, Oklahoma; [2]Department of Pharmacy-Center for Drug Research, Center for Integrated Protein Science Munich (CIPSM), Ludwig-Maximilians-Universität München, Munich, Germany; [3]Research Service, Veterans Administration Western New York Healthcare System, Buffalo, New York; Departments of [4]Ophthalmology (Ira G. Ross Eye Institute/Vision Research Center) and [5]Biochemistry, University at Buffalo/State University of New York, Buffalo, New York; and [6]SUNY Eye Institute, Buffalo, New York.

Supported by NCRR Grant P20 RR017703, NIH/NEI Grants P30 EY12190, R01 EY019490 and R01 EY007361, an unrestricted grant from Research to Prevent Blindness, a research grant from the American Health Assistance Foundation, the Oklahoma Center for the Advancement of Science & Technology (OCAST), and grants from the Deutsche Forschungsgemeinschaft (DFG).

Submitted for publication July 5, 2011; revised October 29 and December 13, 2011; accepted December 30, 2011.

Disclosure: **J. Xu**, None; **L.M. Morris**, None; **S. Michalakis**, None; **M. Biel**, None; **S.J. Fliesler**, None; **D.M. Sherry**, None; **X.-Q. Ding**, None

Corresponding author: Xi-Qin Ding, 940 Stanton L. Young Boulevard, BMSB 553, Oklahoma City, OK 73104; xi-qin-ding@ouhsc.edu.

CNGA1 and CNGB1 subunits, while the cone CNG channel is formed from CNGA3 and CNGB3 subunits. Heterologous expression studies have shown that the A subunits are responsible for the ion-conducting activity of the channel, whereas the B subunits function as modulators.

Mutations in the rod-specific *CNGA1* and *CNGB1* genes are associated with RP,[17,18] while mutations in the cone-specific *CNGA3* and *CNGB3* genes are linked to achromatopsia, cone dystrophy, and some maculopathies.[6,19] Indeed, over 70 disease-associated mutations have been identified in *CNGA3* and *CNGB3*,[6,19–21] and these mutations account for over 70% of achromatopsia patients.[6,22–24] Achromatopsia is a devastating hereditary visual disorder characterized by reduced cone-mediated ERG responses, color blindness, visual acuity loss, pendular nystagmus, extreme light sensitivity, and daytime blindness. As the disease is primarily caused by mutations in CNG channel subunits, achromatopsia is often referred to as a "channelopathy." Cone degeneration in patients with CNG channel deficiency has been documented by optical coherence tomography (OCT) studies.[25–27] Loss of cone function and progressive cone degeneration also has been documented in CNGA3$^{-/-}$ and CNGB3$^{-/-}$ mouse models.[28–30]

The current studies were designed to explore the secondary effects of cone degeneration on rods by characterizing rod function, structural integrity and survival after loss of cones in CNGA3$^{-/-}$ mice, a model for human achromotopsia. CNGA3$^{-/-}$ mice have no detectable cone ERG responses and develop early-onset cone degeneration,[28,29] which is detected as early as the second postnatal week, with complete loss of cones from the ventral retina after the third postnatal month.[29] In this report, we show secondary, age-dependent effects on rod-driven electrophysiological function in CNGA3$^{-/-}$ mice. The scotopic ERG b-wave was reduced as early as 1 month, while a reduced ERG a-wave only appeared much later, at 9 months. We also show a reduced outer nuclear layer (ONL) thickness and reduced expression of rod-specific proteins in CNGA3$^{-/-}$ mice at 12 months. Cone terminals in the CNGA3$^{-/-}$ retina showed a progressive loss of neurochemical and ultrastructural integrity, accompanied by disorganized rod terminal ultrastructure by 12 months. The appearance of scotopic ERG b-wave defects before a-wave deficits, together with the progressive loss of neurochemical and ultrastructural integrity of cone photoreceptor terminals, suggest that compromised CNG channel function and phototransduction lead to early impairment of synaptic terminal function and structural integrity. Our findings also indicate that impaired cone function leads to deleterious secondary effects on rod function, structure, and survival.

Materials and Methods

Mice, Antibodies, and Other Materials

The generation of the CNGA3$^{-/-}$ mouse line (on a C57BL/6 background) was described previously.[28] Wild-type mice (C57BL/6) were purchased from Charles River Laboratories (Wilmington, MA). All mice were maintained under moderately dim cyclic light (12 hours light/12 hours dark) conditions; cage illumination was approximately 7 footcandles (ca. 75 lux) during the light phase of the cycle. All animal experiments were performed at The University of Oklahoma Health Sciences Center (OUHSC) and were approved by the local Institutional Animal Care and Use Committees (OUHSC, Oklahoma City, OK) and conformed to the guidelines on the care and use of animals adopted by the Society for Neuroscience and the Association for Research in Vision and Ophthalmology (Rockville, MD).

Rabbit polyclonal antibody against rhodopsin was kindly provided by Debra Thompson (University of Michigan Medical School, Ann Arbor, MI). Monoclonal antibodies against glutamic acid-rich protein (GARP) and against rhodopsin (1D4) were kindly provided by Robert Molday (University of British Columbia, Vancouver, Canada). Affinity-purified rabbit polyclonal antibodies against mouse M-opsin and cone arrestin (CAR) were kindly provided by Cheryl Craft (University of Southern California, Keck School of Medicine, Los Angeles, CA). Rabbit polyclonal antibodies against rod transducin α-subunit (Gnat1) and cone transducin α-subunit (Gnat2) were obtained from Santa Cruz Biotechnology, Inc. (Santa Cruz, CA). Monoclonal anti-actin antibody was purchased from Abcam, Inc. (Cambridge, MA). Mouse monoclonal antibody directed against C-terminal binding protein 2 (CtBP2) was purchased from BD Transduction Laboratories (San Jose, CA). Rabbit polyclonal anti–complexin 3 was purchased from Synaptic Systems (Göttingen, Germany). Wheat germ agglutinin (WGA) and peanut agglutinin (PNA) conjugated to AlexaFluor-488, or -568, and fluorescent goat anti-mouse and goat anti-rabbit secondary antibodies conjugated to AlexaFluor-488, -568, or -647 were purchased from Invitrogen-Molecular Probes (Carlsbad, CA). Secondary horseradish peroxidase-conjugated anti-rabbit or anti-mouse antibodies were purchased from Kirkegaard & Perry Laboratories Inc. (Gaithersburg, MD). All other chemicals were purchased from Sigma-Aldrich (St. Louis, MO), Bio-Rad (Hercules, CA), or Invitrogen (Carlsbad, CA).

Evaluation of Rod and Rod-Driven Function by ERG Recordings

Full-field ERG testing was carried out as described previously.[30,31] Briefly, after overnight dark adaptation, animals were anesthetized by intraperitoneal injection of 85 mg/kg ketamine and 14 mg/kg xylazine. ERGs were recorded (LKC system, Gaithersburg, MD). Potentials were recorded using a platinum wire contacting the corneal surface through a layer of 2.5% methylcellulose. For assessment of scotopic responses, a white light stimulus intensity of 1.89 log cd s m^{-2} was presented to dark-adapted, dilated mouse eyes in a Ganzfeld (GS-2000; Nicolet Instruments, Inc., Madison, WI). Age-matched CNGA3$^{-/-}$ and wild-type mice at 1, 3, 6, 9, and 12 months were analyzed. In a separate experiment to examine the light responses to a broad range of stimulus intensities, groups of CNGA3$^{-/-}$ and wild-type mice at 1 and 12 months were analyzed using stimuli with intensities ranging from −3.6 to 2.1 log cd s m^{-2}. To evaluate photopic responses, mice were adapted to a 1.46 log cd s m^{-2} light for 5 minutes, and then a light intensity of 1.89 log cd s m^{-2} was given.[32,33] Responses were differentially amplified, averaged, and stored using a signal averaging system (Nicolet Compact-4; Nicolet Biomedical Instruments, Madison, WI). The ERG testing was performed between 10:00 AM and 12:00 PM.

Evaluation of Retinal Structure by Light Microscopy and Morphometric Analysis

Euthanasia of mice was performed by CO_2 asphyxiation and eye samples were prepared for light microscopy as described previously.[30,34] Briefly, mouse eyes were enucleated and fixed with 4% formaldehyde in 0.1 M sodium phosphate buffer, pH 7.4 for 16 hours at 4°C. The superior portion of the cornea was marked with a green dye for orientation before enucleation. Fixed eyes were transferred to PBS or 0.1 M sodium phosphate buffer, pH 7.4, containing 0.02% sodium azide, for storage until processing and embedding in paraffin. For morphometric analysis by quantitative histology, 5 μm thick sections of retinas were cut along the vertical meridian passing through the optic nerve head and stained with hematoxylin and eosin (H&E) to allow an examination of the retina in the superior and inferior hemispheres. In each hemisphere, ONL thickness was measured at 0.24 mm intervals in nine defined areas, starting at the optic nerve head and extending along the vertical meridian toward the superior and inferior ora serrata.[35] Mean ONL thickness at the inferior and superior locations was then calculated. In each experimental group, two to three sections from each of the retinas of three to four mice were measured.

To assess the proportion of the ONL occupied by cones, paraffin-embedded sections of wild-type and CNGA3$^{-/-}$ retinas were immunolabeled for CtBP2, a marker for cone cell bodies, and PNA, a specific

marker for interphotoreceptor matrix surrounding the outer and inner segments of cones, and mounted with medium containing DAPI (Prolong Gold; Invitrogen-Molecular Probes) to visualize nuclear structure as described above. Matching images containing the ONL were captured at magnification ×40 in all three labeling channels, scale was calibrated, and the images were imported into ImageJ (developed by Wayne Rasband, National Institutes of Health, Bethesda, MD; available at http://rsb.info.nih.gov/ij/index.html) for analysis. PNA labeling and the structure of DAPI labeling were used to confirm the identity of the CtBP2-positive cells as cones (see Results). The borders of the ONL were traced on the DAPI image using the polygon selection tool to create a region of interest corresponding specifically to the ONL and the total area of the ONL was measured. To determine the area occupied specifically by cones, the CtBP2 image was thresholded to specifically highlight labeling in cone cell bodies, and the total thresholded area within the ONL region of interest selected on the DAPI image was measured. To determine the proportion of the ONL occupied by cones, the area occupied by CtBP2-positive cones was divided by the total area of the ONL determined from the DAPI image and expressed as a percentage.

Evaluation of Expression of Rod- and Cone-Specific Proteins by Western Blot Analysis

Protein SDS-PAGE and Western blot analysis were performed as described previously.[30,31] Briefly, retinas were homogenized in homogenization buffer (10 mM Tris-HCl, pH 7.4, 1 mM EDTA, 200 mM sucrose, 1 mM phenylmethylsulfonyl fluoride). The nuclei and cell debris were removed from the homogenate by centrifugation at 1000*g* for 10 minutes at 4°C. The resulting supernatant was centrifuged at 16,000*g* for 30 minutes at 4°C. The resultant membranes were used in Western blot analysis.

Retinal membrane proteins were separated by SDS-PAGE and transferred onto polyvinylidene diflouride membranes. After 1 hour of blocking in 5% nonfat milk at room temperature, blots were incubated with primary antibody (anti-rhodopsin, 1:5000; anti-GARP, 1:500; anti-Gnat1, 1:500; anti–M-opsin, 1:2000; anti-Gnat2, 1:500; anti-CAR, 1:2000; or anti-actin, 1:5000) overnight at 4°C. After rinsing in Tris-buffered saline with 0.1% Tween 20, blots were incubated with HRP-conjugated secondary antibodies (at 1:5000 for anti-actin and anti-GARP; 1:25,000 for other antibodies) for 1 hour at room temperature. Chemiluminescent substrate (SuperSignal West Dura Extended Duration; Pierce, Rockford, IL) was used to detect binding of the primary antibodies to their cognate antigens. The Western blot analyses were scanned and images were captured using a digital imaging system (Kodak Image Station 4000R; Carestream Molecular Imaging, New Haven, CT). Densitometry analysis was performed by quantifying the intensities of the bands of interest using software (Kodak Molecular Imaging software version 4.0; Carestream Molecular Imaging) with β-actin serving as a (loading) control. The results for each group were obtained from three to four independent Western blot experiments using retinas prepared from four to five mice.

Evaluation of Photoreceptor Synaptic Terminal Integrity by Antibody and Lectin Labeling

To assess the integrity of photoreceptor synaptic terminals, wild-type and CNGA3$^{-/-}$ mouse eyes were fixed and embedded in paraffin as described above, sectioned at a thickness of 5 μm, and immunolabeled as described previously.[34,36] Cone terminals were identified using a rabbit polyclonal antibody against complexin 3 (1:1000). Synaptic ribbons were labeled using a mouse monoclonal antibody directed against CtBP2 (1:1000). WGA conjugated to AlexaFluor-488 (1:40) was used to assess the arrangement of rod and cone terminals in the OPL. PNA conjugated to AlexaFluor-568 (1:20) was used to identify the sheath surrounding cone outer segments and flat contacts between cone terminals and OFF-cone bipolar cell dendrites. To assess the integrity of rods, labeling for rod opsin was performed using monoclonal antibody 1D4 (1:50). Binding of primary antibodies was visualized using an appropriate combination of goat anti-mouse and goat anti-rabbit secondary antibodies conjugated to AlexaFluor-488, -568, or -647 (diluted 1:200–1:500). Labeled sections were mounted using mounting medium containing DAPI (Prolong Gold; Invitrogen-Molecular Probes) to retard bleaching and visualize nuclei. Imaging was performed using an epifluorescence microscope (BX61-WI; Olympus America, Center Valley, PA) fitted with a digital camera (ORCA-ER; Hamamatsu, Bridgewater, NJ) and controlled by software (Slidebook version 4.0.2.8; Intelligent Imaging Innovations, Denver, CO). Figures were prepared by calibrating image scale, exporting images to image-processing software (Photoshop version 7.0; Adobe, Mountain View, CA) and adjusting brightness, contrast, and threshold to highlight specific labeling.

Evaluation of Photoreceptor Outer Segment and Synaptic Terminal Ultrastructure by Transmission Electron Microscopy

Mouse eyes were prepared for transmission electron microscopy as described previously.[30,31] Tissue sections were obtained with a microtome (Reichert-Jung Ultracut E Microtome; American Instrument, Haverhill, MA) using a diamond knife. Thin (600–800 Å) sections were collected on copper 75/300 mesh grids for conventional EM analysis and stained with 2% (wt/vol) uranyl acetate and Reynolds' lead citrate to examine the ultrastructural organization of rod and cone outer segments, terminals, and their synapses. Sections were viewed with an electron microscope (JEOL 100CX; JEOL USA Inc., Peabody, MA) at an accelerating voltage of 60 keV, and digital images were collected and stored on a computer for subsequent viewing and analysis.

Statistical Analysis

One-way ANOVA (Newman-Keuls multiple comparison test) or unpaired Student's *t*-test were used to determine statistical significance ($^*P < 0.05$). Statistical analyses were performed using software (GraphPad Prism, version 5.0 for Windows; GraphPad Software, San Diego, CA).

Results

Impaired Rod ERG Responses in CNGA3$^{-/-}$ Mice

To determine whether rod function in CNGA3$^{-/-}$ mice was affected, we performed scotopic ERG recordings at 1, 3, 6, 9, and 12 months of age and found an age-dependent reduction of the ERG a- and b-wave amplitudes in CNGA3$^{-/-}$ mice compared with age-matched wild-type controls. Figure 1A shows scotopic a- and b-wave amplitude in response to stimuli at an intensity of 1.89 log cd s m^{-2} in CNGA3$^{-/-}$ and wild-type mice at varying ages. There were no statistically significant differences in the ERG a-wave amplitude between CNGA3$^{-/-}$ and wild-type mice at 1, 3, or 6 postnatal months. However, at 9 and 12 months, the a-wave amplitude in CNGA3$^{-/-}$ mice was reduced by approximately 20%, compared with age-matched wild-type controls (Fig. 1A, left panel). In contrast, reduced ERG b-wave amplitude was evident in CNGA3$^{-/-}$ mice as early as 1 month, with a 15% reduction at 1 month, 30% at 6 months, and 40% at 9 and 12 months (Fig. 1A, right panel). These studies suggested that rod function might be impaired. To better assess effects of CNGA3 deficiency on rod-driven signals, we performed ERG recordings in CNGA3$^{-/-}$ and wild-type mice at 1 and 12 months of age using stimuli at increasing intensities over the entire scotopic range. Figure 1B illustrates representative scotopic ERG recordings from CNGA3$^{-/-}$ and wild-type mice. As reported previously,[28] there were no differences in a-wave amplitudes between CNGA3$^{-/-}$ and wild-type mice at 1 month at any stimulus intensity (Figs. 1B, 1C). However, a-wave amplitudes in 12-month-old CNGA3$^{-/-}$ mice were significantly decreased at stimulus intensities of 0.86 log cd s m^{-2} or more (Figs. 1B, 1C), indicating that rod function

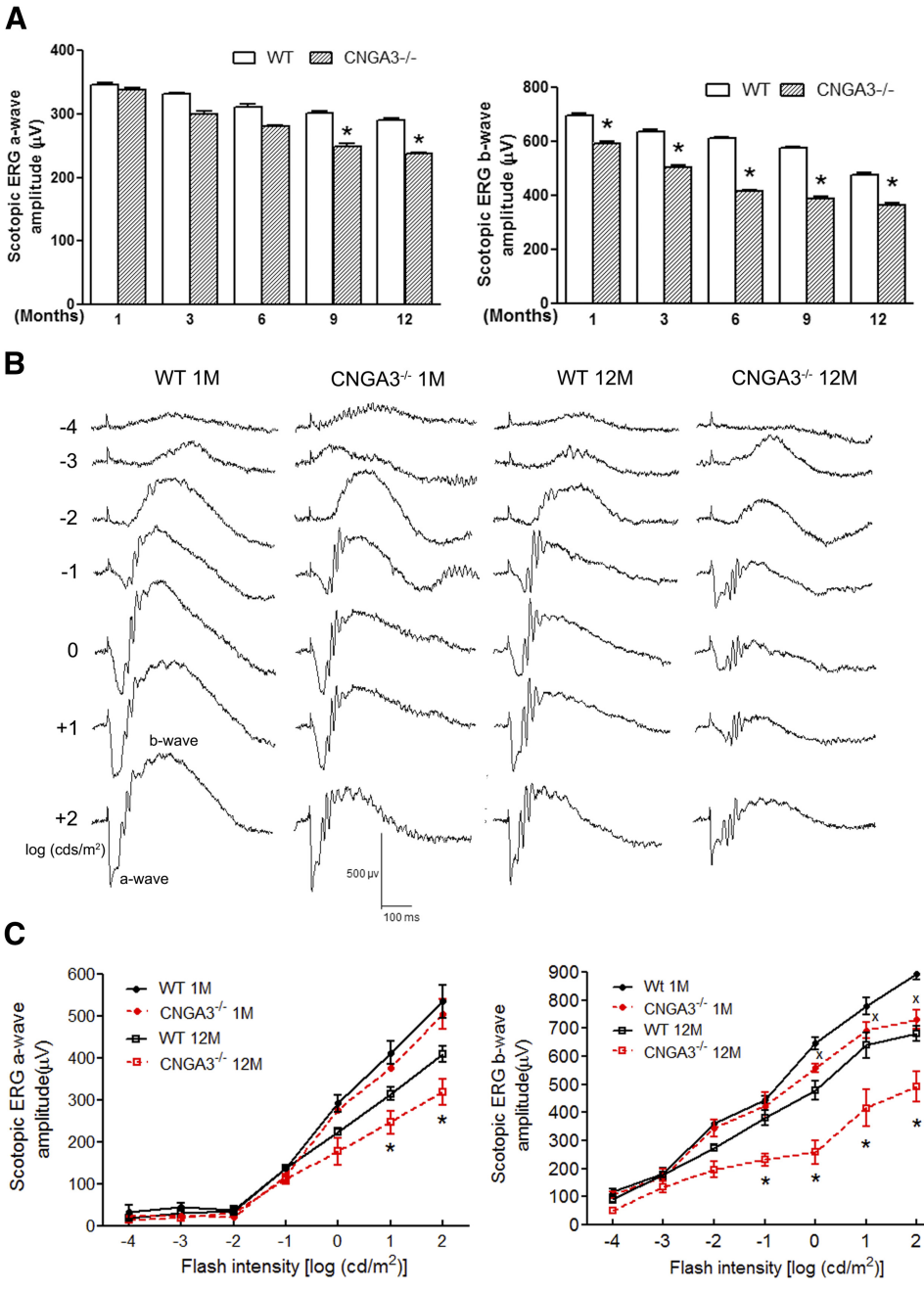

Figure 1. Impaired rod and rod-driven ERG responses in CNGA3$^{-/-}$ mice. Scotopic ERG recordings were performed in CNGA3$^{-/-}$ and wild-type (WT) mice at varying postnatal ages, from 1 to 12 months. (**A**) Scotopic a-wave (*left*) and b-wave (*right*) amplitude in CNGA3$^{-/-}$ and WT mice. Data are represented as mean ± SEM (n = 8 to 12 mice for each group) (*$P < 0.05$). (**B**). Representative waveforms of scotopic ERG recordings to serial stimuli at increasing intensities from CNGA3$^{-/-}$ and WT mice at 1 and 12 months. (**C**). Scotopic ERG a-wave (*left*) and b-wave (*right*) amplitude in response to stimulus of increasing intensity from CNGA3$^{-/-}$ and WT mice at 1 and 12 months. Data are represented as mean ± SEM (n = 4 to 5 mice for each group) (*$P < 0.05$, compared with WT mice at 12 months; X, $P < 0.05$, compared with WT mice at 1 month).

was impaired by 12 months of age. We also examined the ERG b-wave to assess whether CNGA3 deficiency also might affect processing of rod-driven signals in the inner retina. The b-wave amplitudes in CNGA3$^{-/-}$ mice were reduced compared with age-matched wild-type controls at both 1 and 12 months of age at stimulus intensities of −0.03 log cd s m^{-2} and greater (Figs.

Figure 2. Reduced ONL thickness in CNGA3$^{-/-}$ mice. Retinal histology and morphometric analysis were performed on retinal cross-sections prepared from CNGA3$^{-/-}$ and WT mice at 1, 6, 9, and 12 months. (**A**) Representative histologic sections through the superior retina near the optic nerve head are shown. GL, ganglion cell layer; INL, inner nuclear layer; IPL, inner plexiform layer; OS, outer segment. Scale bar, 50 μm for all panels. (**B**) Quantification of ONL thickness measurements. Measurements of ONL thickness were performed at 0.24 mm intervals from the optic nerve head along the vertical meridian in the superior and inferior regions of the retinas. *Insets* show mean ONL thickness in the inferior and superior regions in CNGA3$^{-/-}$ and WT mice at 12 months. Data are represented as mean ± SEM (n = 3 to 4 mice for each group) (*$P < 0.05$). (**C**) Evaluation of proportion of the ONL occupied by cones. *Top*: electron micrograph (*leftmost panel*). Large cone nuclei (c) display several patches of electron dense euchromatin. Rod nuclei (r) are smaller and dominated by a large electron dense core of euchromatin. CIS, cone inner segment; RIS, rod inner segment. Scale bar, 2 μm. At the light microscopic level, cones can be distinguished from rods by their nuclear structure and CtBP2 labeling (*remaining top panels*). Wild-type retina at 1 month of age was shown. Labeling for CtBP2 is found in a subset of photoreceptor cell bodies (*arrowheads*) corresponding to PNA-labeled cones. Rod cell bodies (*arrows*) do not show CtBP2 labeling. Cone nuclei show multiple patches of intense DAPI labeling. Rod nuclei show a dense core of DAPI labeling. Scale bars, 10 μm. IS, inner segment. *Bottom*: quantification of proportion of ONL occupied by cones determined from CtBP2 labeling. Data represent mean ± SEM (n = 3 to 4 mice for each group) (*$P < 0.05$).

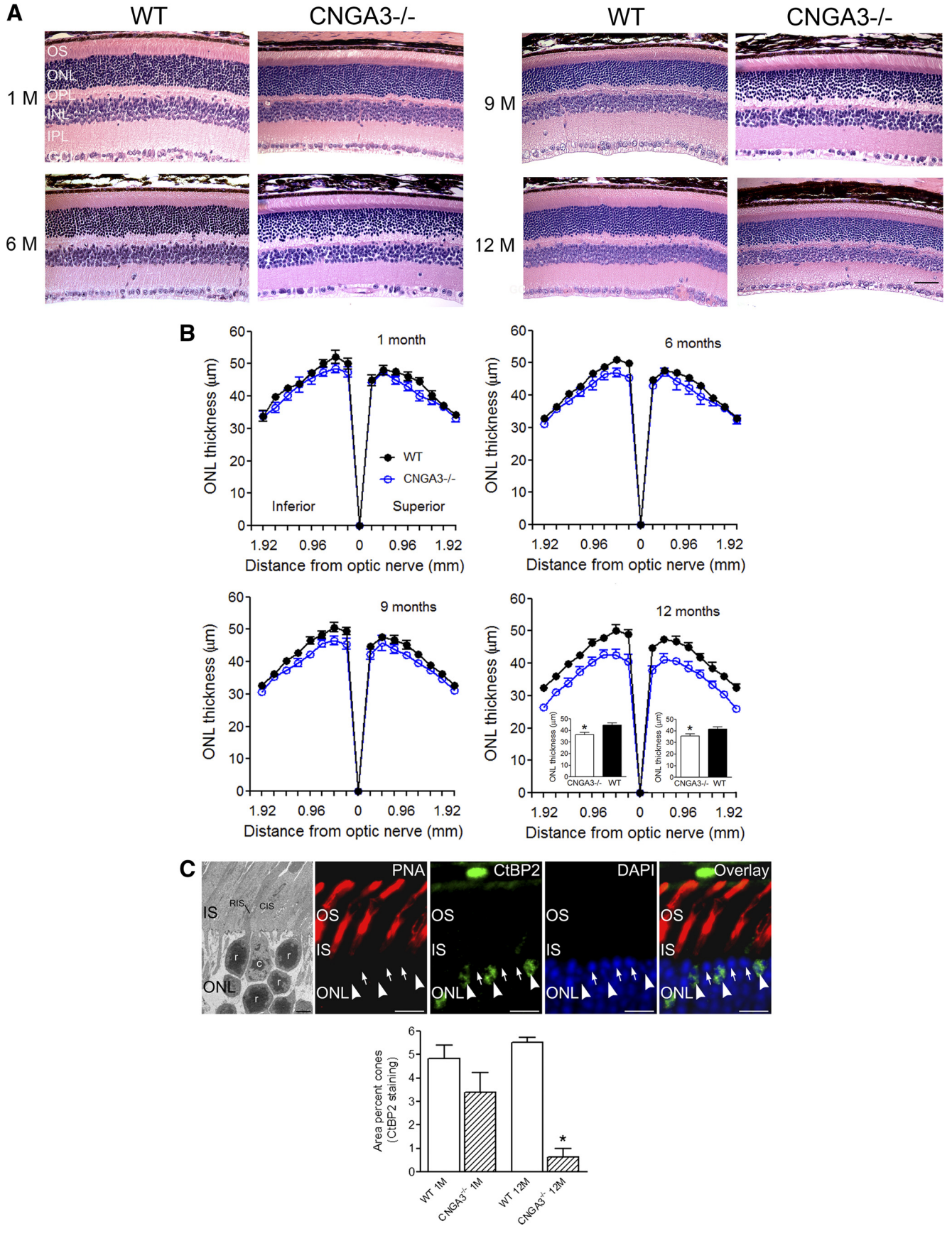
A
WT
CNGA3-/-
WT
CNGA3-/-
OS
ONL
OPL
INL
IPL
1 M
9 M
6 M
12 M
B
1 month
6 months
9 months
12 months
ONL thickness (µm)
Distance from optic nerve (mm)
WT
CNGA3-/-
Inferior
Superior
1.92
0.96
0
0.96
1.92
C
PNA
CtBP2
DAPI
Overlay
IS
RIS
CIS
ONL
OS
Area percent cones (CtBP2 staining)
WT 1M
CNGA3-/- 1M
WT 12M
CNGA3-/- 12M

1B, 1C). By 12 months of age, the reduction in b-wave amplitudes became much more pronounced, and were significantly lower than those obtained from age-matched wild-type controls at intensities of -0.99 log cd s m^{-2} or greater (Figs. 1B, 1C). Thus, postphotoreceptoral neurons showed reduced scotopic ERG b-wave as early as 1 month of age, although the responses of the rods themselves were not affected until approximately 9 months in CNGA3$^{-/-}$ mice. The ERG a- and b-wave response amplitudes to 1.89 log cd s m^{-2} stimuli in the serial ERG recordings (Fig. 1C) tended to be higher than the responses recorded at the same intensity in the single stimulus recordings (Fig. 1A). The reason for this difference is not obvious, but may reflect adaptive changes in response to serial stimuli. Cone responses were absent in the CNGA3$^{-/-}$ mice as we reported previously.[28]

Reduced ONL Thickness and Rod-Specific Protein Expression Levels in CNGA3$^{-/-}$ Mice

To evaluate rod survival in CNGA3$^{-/-}$ mice, we examined retinal structure at 1, 6, 9, and 12 months using light microscopy and morphometric analysis (Fig. 2). The histologic appearance of CNGA3$^{-/-}$ and wild-type mice was comparable at 1, 6, and 9 months. However, at 12 months outer segment length and ONL thickness (and number of rows of photoreceptor nuclei) were reduced in CNGA3$^{-/-}$ mice compared with age-matched wild-type controls (Fig. 2A). Some additional thinning also may have been present in the CNGA3$^{-/-}$ inner retina, as the INL and IPL, and possibly the GCL, appeared to be reduced in thickness at 9 and 12 months, compared with age-matched wild-type retina. Thus, in the aged CNGA3$^{-/-}$ retina it is possible that some neurons also may be lost from the inner retina. Figure 2B shows the quantitative analysis of ONL thickness in CNGA3$^{-/-}$ and wild-type mice at 1, 6, 9, and 12 months. ONL thickness did not differ between CNGA3$^{-/-}$ and wild-type mice at 1, 6, or 9 months, but the average ONL thickness in CNGA3$^{-/-}$ mice at 12 months was reduced by approximately 15% in both the superior and inferior retina compared with age-matched wild-type controls (see insets, Fig. 2B).

To determine whether the loss of cones alone could account for the magnitude of the observed decrease in ONL thickness in the CNGA3$^{-/-}$ retina, we estimated the proportion of space in the ONL occupied by cones in CNGA3$^{-/-}$ and wild-type retinas at 1 and 12 months of age. Cones and rods can be distinguished by their nuclear architecture and marker labeling. At the electron microscopic level, cones have large nuclei containing several small patches of euchromatin surrounded by abundant heterochromatin. In contrast, rod nuclei are smaller and show a large dense core of euchromatin surrounded by a thin rim of heterochromatin (Fig. 2C, leftmost panel). These characteristics can be visualized for analysis of cones at the light microscopic level. CtBP2, a transcription factor, selectively labels a set of cells with the characteristic placement of cones. Triple labeling for CtBP2 together with DAPI to visualize chromatin structure and PNA to identify cone outer and inner segments, confirmed that CtBP2 selectively labeled cones (Fig. 2C, remaining top panels). In comparison, the smaller rod cell bodies lacked CtBP2 labeling and showed a single dense DAPI-positive core of euchromatin. To quantify the proportion of the ONL occupied by cone cells in the wild-type and CNGA3$^{-/-}$ retina at 1 and 12 months of age, we analyzed CtBP2 immunolabeling in the ONL of retinas labeled for CtBP2 and DAPI. The total area of the ONL was measured from the DAPI image, the total area occupied by cones was determined by measuring the area within the ONL occupied by CtBP2 labeling, and the proportion of the ONL occupied by cones was determined. At 1 and 12 months of age, cones occupied approximately 5% of the space in the ONL in the wild-type retina. In the CNGA3$^{-/-}$ retina, a decrease in cones was detectable by 1 month of age, although it did not achieve statistical significance. Severe cone loss was evident by 12 months ($P = 5.3 \times 10^{-7}$, compared with 12-month-old wild-type, Fig. 2C, bottom panel). These findings show that the loss of cones alone, which occupy approximately 5% of the area of the ONL in vertical sections of the healthy wild-type retina, cannot account for all the observed thinning of the ONL in the CNGA3$^{-/-}$ retina, which is reduced by approximately 15% in central retina at 12 months of age (Fig. 2B). Thus, additional (noncone) cells must be lost from the ONL, most likely rods.

To further evaluate rod integrity, we performed Western blot analysis to assess the expression levels of rod-specific proteins, including rhodopsin, Gnat1, and GARP in CNGA3$^{-/-}$ and wild-type mouse retinas at 1 and 12 months of age (Fig. 3A). Rhodopsin, Gnat1, and GARP levels were all somewhat lower in CNGA3$^{-/-}$ than in wild-type retinas at one postnatal month, before the appearance of measurable rod loss; these differences, however, were not statistically significant. In contrast, the expression levels of rhodopsin, Gnat1, or GARP all were significantly reduced (*P*-values: 0.021, 0.026, and 0.012, respectively) in CNGA3$^{-/-}$ compared with age-matched wild-type retinas at 12 months. The expression levels of rhodopsin, Gnat1, and GARP in CNGA3$^{-/-}$ mouse retinas at 12 months were reduced by 37%, 30%, and 42%, respectively, compared with age-matched controls (Figs. 3B–D). Hence, significant reductions in rod-specific protein levels correlated with rod degeneration in CNGA3$^{-/-}$ mice, as measured by reduced ONL thickness.

We also compared expression levels of cone-specific proteins in CNGA3$^{-/-}$ and age-matched wild-type control mouse retinas at 1 and 12 months to determine how CNGA3 deficiency affected the expression of proteins specifically associated with cone phototransduction. Western blot analysis was performed to examine the expression of M-opsin, Gnat2, and CAR (Fig. 4A). Levels of all these cone-specific phototransduction proteins in CNGA3$^{-/-}$ mouse retinas were significantly reduced as early as one postnatal month compared with age-matched wild-type mouse retinas (Figs. 4B–D). A further reduction in the levels of these proteins was seen in CNGA3$^{-/-}$ mice at 12 months, compared with both age-matched wild-type mice and to the levels observed in CNGA3$^{-/-}$ mice at 1 month. Densitometric analysis showed that the levels of M-opsin, Gnat2, and CAR in CNGA3$^{-/-}$ mouse retinas at 12 months were approximately 5%, 10%, and 14%, respectively, of the levels in the age-matched controls, and approximately 20%, 35%, and 43%, respectively, of the levels in CNGA3$^{-/-}$ mouse retinas at 1 month (Figs. 4B–D).

Disrupted Rod Outer Segment Ultrastructure in CNGA3$^{-/-}$ Mice

Disrupted cone outer segment (COS) ultrastructure in CNGA3$^{-/-}$ mice has been described previously.[28] To test whether CNGA3 deficiency also affected rod outer segment (ROS) structure, we assessed rod outer segment ultrastructure by transmission electron microscopy in CNGA3$^{-/-}$ and age-matched wild-type mice at 1 and 12 postnatal months. Wild-type mice at 1 and 12 months and CNGA3$^{-/-}$ mice at 1 month showed normal ROS ultrastructure, but disorganized ROS and disc ultrastructure was observed in CNGA3$^{-/-}$ mice at 12 months. ROSs in the wild-type and 1-month-old CNGA3$^{-/-}$ retina had normal ultrastructure with tightly packed, flattened discs and the characteristic hairpin structure of the disc rim. However, ROS organization was disrupted in CNGA3$^{-/-}$ mice at 12 months, with irregular packing of discs, enlarged spaces between discs and

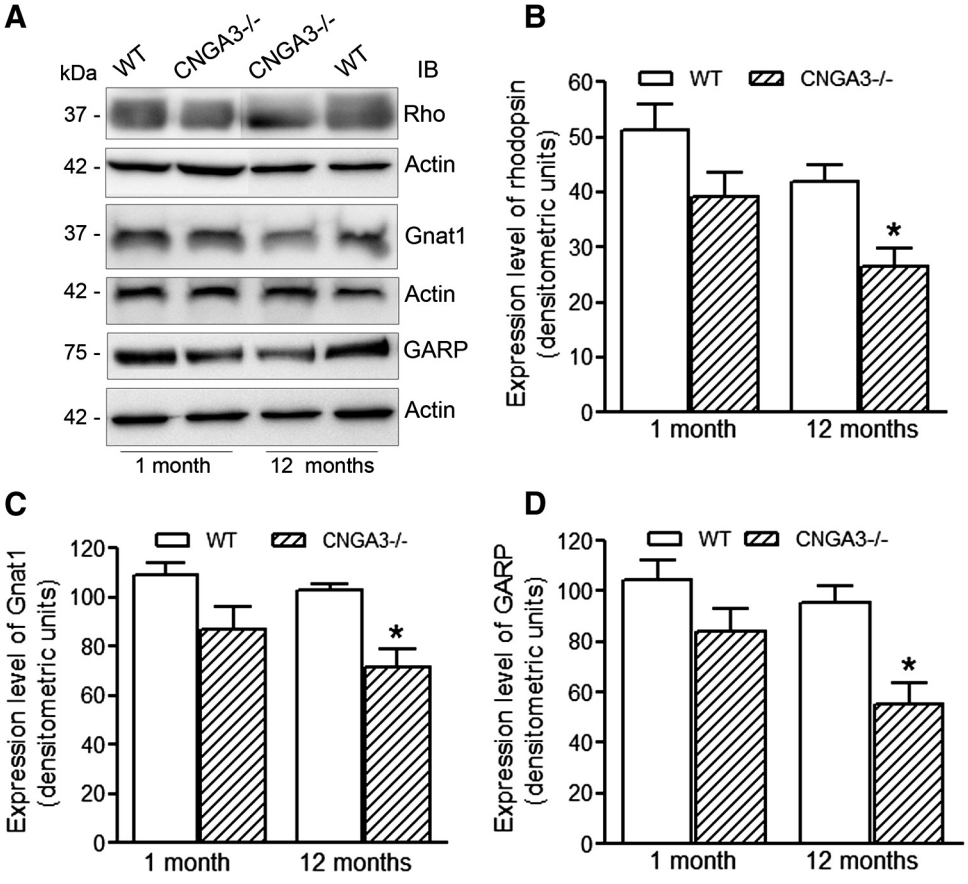

FIGURE 3. CNGA3$^{-/-}$ mice show reduced expression of rod-specific proteins. Western blot detection was performed using retinal membrane protein extracts prepared from CNGA3$^{-/-}$ and WT mice at 1 and 12 postnatal months to assess expression of rhodopsin, Gnat1, and GARP. Actin was included as a loading control. (**A**) Representative images of Western blot detection. Rho, rhodopsin. Densitometric analysis of Western blot detection of rhodopsin (**B**), Gnat1 (**C**), and GARP (**D**). Data are represented as mean ± SEM of measurements from three to four independent experiments using retinas from four to six mice (*$P < 0.05$).

disrupted hairpin structure at the disc margin. Figure 5 shows representative images of the ROS structure in CNGA3$^{-/-}$ and wild-type mice at 1 (Figs. 5A, 5B) and 12 months (Figs. 5C, 5D) at relatively low magnification and the details of disc structure at higher magnification, respectively (Figs. 5A*, 5B*, 5C*, 5D*).

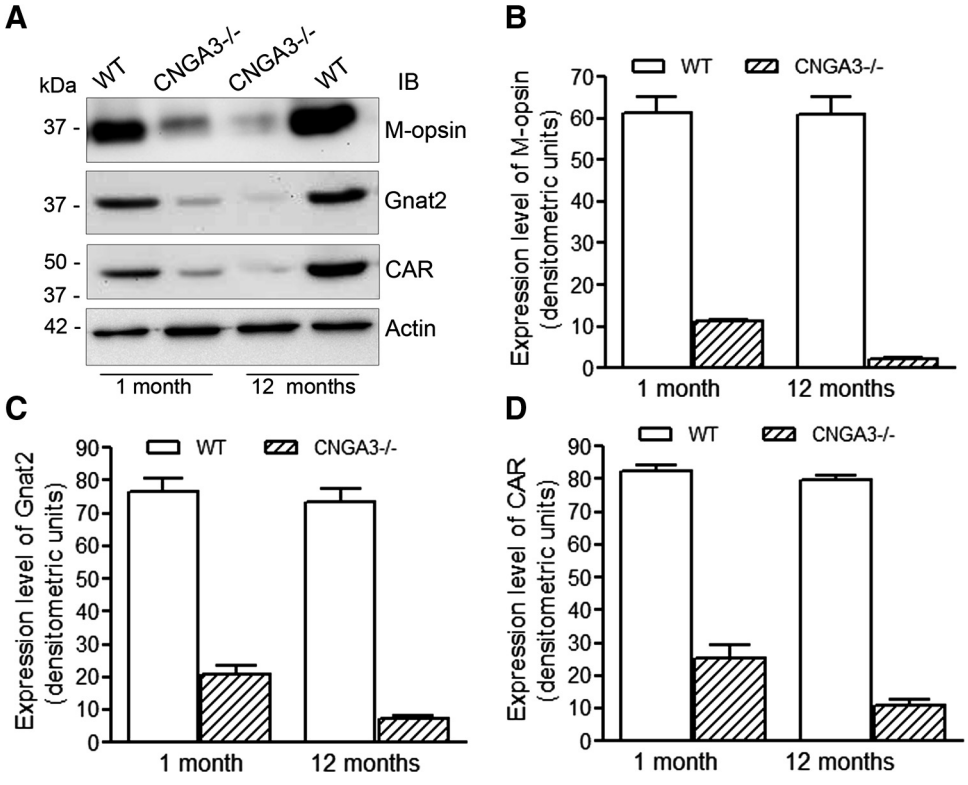

FIGURE 4. CNGA3$^{-/-}$ mice show reduced expression of cone-specific proteins. Western blot detection was performed using retinal membrane protein extracts prepared from CNGA3$^{-/-}$ and WT mice at 1 and 12 months to determine the expression of M-opsin, Gnat2, and CAR. Actin was included as a loading control. (**A**) Shown are the representative images of Western blot detection. Densitometric analysis of Western blot detection of M-opsin (**B**), Gnat2 (**C**), and CAR (**D**). Data are presented as mean ± SEM of measurements from four to five independently performed experiments using retinas from four to six mice (*$P < 0.05$).

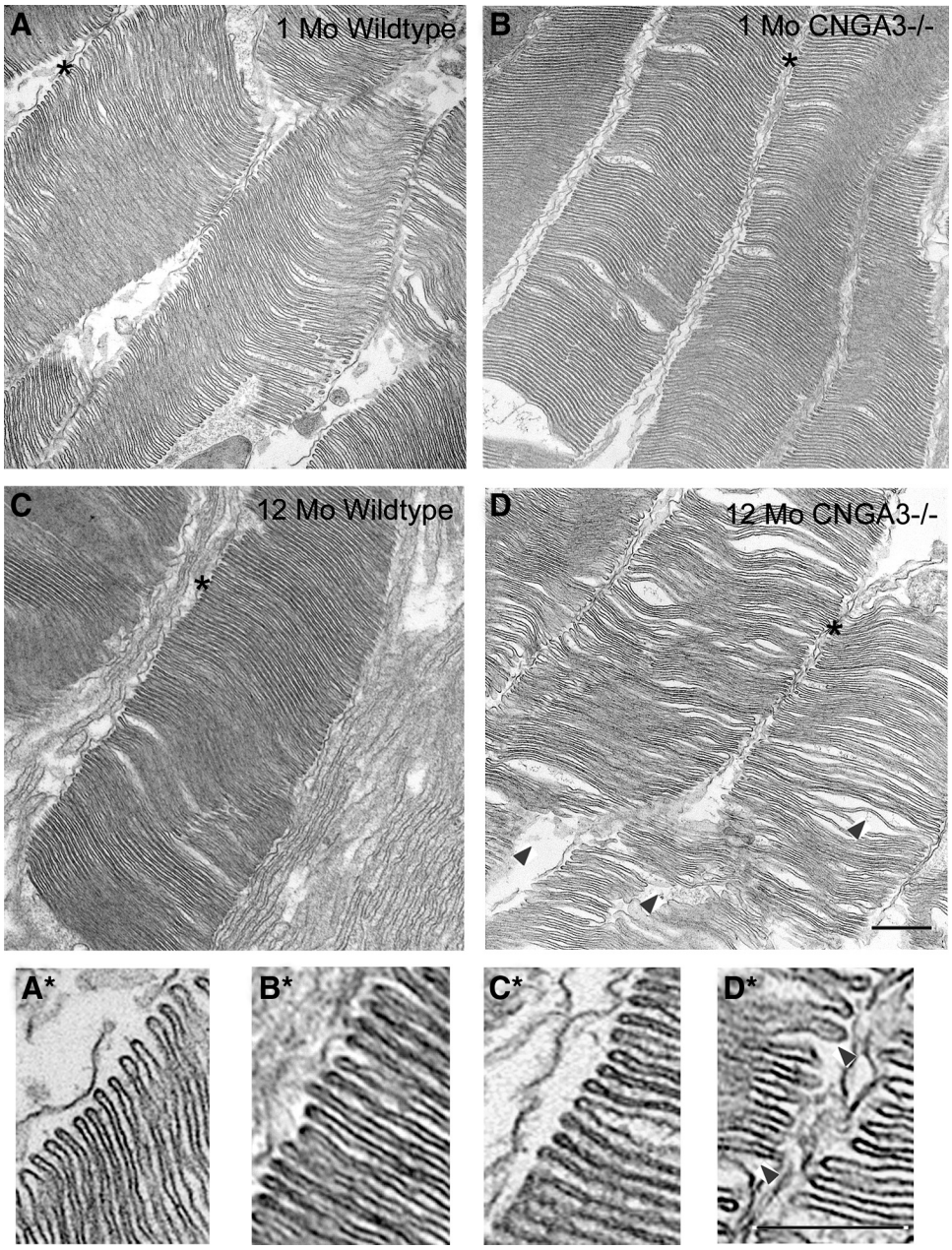

FIGURE 5. Disorganization of rod outer segment ultrastructure in CNGA3$^{-/-}$ mice. Transmission electron microscopy was performed on retinal sections prepared from CNGA3$^{-/-}$ and wild-type mice. Shown are representative images taken at 1 (**A**, **B**) and 12 (**C**, **D**) months. (**A***), (**B***), (**C***), and (**D***) are higher magnification images of the regions marked with an *asterisk* in (**A**–**D**), respectively. Rod outer segments (ROSs) in the WT retina have normal ultrastructure with tightly packed and flattened discs, while disorganization of ROSs was observed in CNGA3$^{-/-}$ mice at 12 months. *Arrowheads* denote disorganized disc arrangement and disrupted ROS ultrastructure. Scale bars, 500 nm for all panels.

Progressive Disorganization of Photoreceptor Terminals in CNGA3$^{-/-}$ Mice

To test whether alterations in cone and rod synaptic terminals might contribute to the functional deficits observed in the ERG recordings from CNGA3$^{-/-}$ mice, we assessed the integrity of photoreceptor terminals by labeling retinal sections from age-matched CNGA3$^{-/-}$ and wild-type mice at 1 and 12 months of age for photoreceptor terminal markers (Fig. 6). Cone terminals were easily identified by their wide spacing and large size compared with the tightly packed, smaller rod terminals in the OPL in wild-type and CNGA3$^{-/-}$ retina at 1 and 12 months of age. However, disruption of cone terminals and the OPL was evident in the CNGA3$^{-/-}$ retina even by 1 month of age. Also by 1 month, cone terminals in the CNGA3$^{-/-}$ retina already showed irregular spacing, reflecting the loss of cones known to occur in CNGA3 deficiency.[29] Some cone terminals showed reduced labeling for the cone-specific presynaptic protein, complexin III, by 1 month of age, suggesting an early decline of neurochemical integrity. However, these cone terminals still retained clusters of synaptic ribbons at their base, identified by CtBP2 labeling, as appropriate. As expected, rod terminals also possessed synaptic ribbons in both CNGA3$^{-/-}$ and wild-type retina at 1 month. By 12 months, large expanses of OPL in the CNGA3$^{-/-}$ retina were devoid of cone terminals, consistent with the known progressive loss of cones.[29] Surviving cone terminals in the 12-month-old CNGA3$^{-/-}$ retina showed a further decrease in complexin III labeling and often showed synaptic ribbons that appeared to be free-floating within the terminal. Synaptic ribbons were still present in surviving rod terminals in the 12-month-old CNGA3$^{-/-}$ retina. In addition, pronounced migration of cells with rod-like nuclear structure into the OPL was noted in the CNGA3$^{-/-}$ retina at 12 months of age (Figs. 6Q–T). Age-matched wild-type retina showed only limited encroachment of cells along the distal edge of the OPL. Immunolabeling for rod opsin, which labels the outer segments and to a lesser extent the plasma membrane of rod cells,

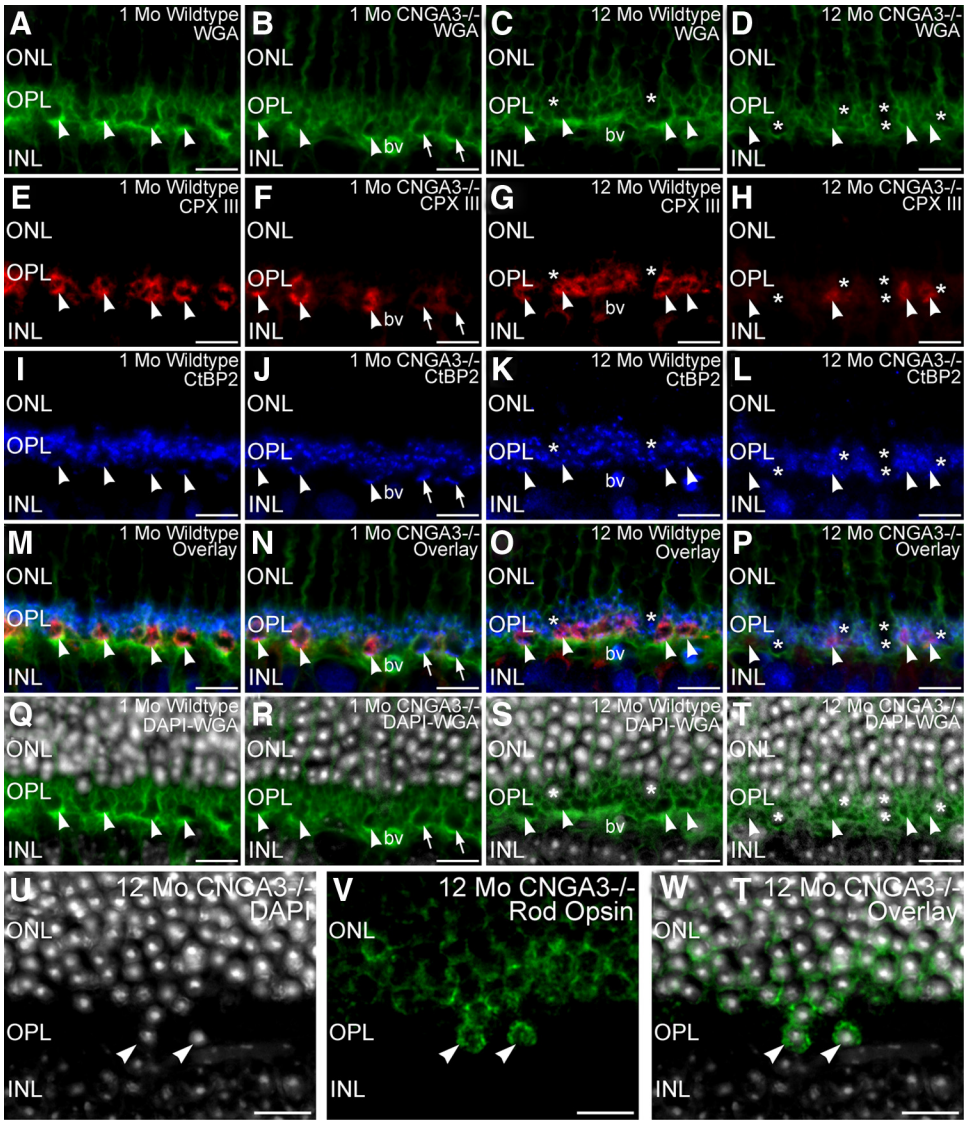

Figure 6. The absence of CNGA3 perturbs cone terminals and OPL organization. Retinas from WT and CNGA3$^{-/-}$ mice at 1 month and 12 months of age labeled with WGA (*green*, **A–D**), complexin III (CPX III; *red*, **E–H**), and CtBP2 (*blue*, **I–L**) to visualize photoreceptor terminal distribution, cone terminals, and synaptic ribbons, respectively. WGA labeling reveals the large terminals of cones (*arrowheads*) and the smaller terminals of rods in the OPL. Cone terminals showed strong labeling for CPX III in the WT retina, but surviving cone terminals in the CNGA3$^{-/-}$ retina often showed reduced or no CPX III labeling (*arrows*, **F**). Synaptic ribbons labeled for CtBP2 were present in rod and cone terminals in all specimens, with cone terminals showing distinct clusters of ribbons at their base in WT and 1-month-old CNGA3$^{-/-}$ retina (**I–K**). Comparable clusters of ribbons were not evident in cone terminals of the 12-month-old CNGA3$^{-/-}$ retina (**L**). (**M–P**) WGA/CPX III/CtBP2 overlay images. (**Q–T**) WGA (*green*) and DAPI (*gray*) labeling of the same sections to illustrate migration of nuclei into the OPL of the CNGA3$^{-/-}$ retina. (**U–W**) show double labeling for DAPI (*gray*) and rod opsin (*green*) in the OPL of CNGA3$^{-/-}$ retina at 12 months of age. Cells invading the OPL (*arrowheads*) show the nuclear structure typical of rod cells (**U**) and labeling for rod opsin (**V**), identifying the cells as rods. Overlay of DAPI and rod opsin labeling (**W**). WT mouse retina shown at one postnatal month (**A, E, I, M, Q**) and 12 months of age (**C, G, K, O, S**). CNGA3$^{-/-}$ mouse retina shown at 1 month (**B, F, J, N, R**) and 12 months of age (**D, H, L, P, T, U–W**). bv, blood vessel. Scale bar, 10 μm for all panels.

in conjunction with DAPI to visualize nuclear structure confirmed that the cells invading the OPL in the 12-month-old CNGA3$^{-/-}$ retina were rods (Figs. 6U–W). Together, these findings suggest a progressive loss of cone terminal integrity followed by secondary effects on rod terminals. The loss of synaptic integrity is accompanied by progressive degradation of OPL organization and migration of rod cell bodies into the OPL. These results are consistent with the progressive loss of rod-driven function observed in the ERG studies.

To further assess synaptic integrity in the absence of CNGA3, we examined the synaptic ultrastructure of cone and rod terminals in wild-type and CNGA3$^{-/-}$ retinas at 1 and 12 postnatal months (Fig. 7). Cone terminals showing normal synaptic ultrastructure were present in both wild-type and CNGA3$^{-/-}$ retina at 1 month of age. These terminals showed multiple synaptic ribbons anchored to the plasma membrane, abundant synaptic vesicles presynaptically, and a "triad" of processes from horizontal and bipolar cells postsynaptically. Flat contacts with OFF-cone bipolar cell dendrites were present along the base of cone terminals. However, cone terminals showing abnormal organization of ribbon synaptic complexes and ribbons that appeared to be free-floating in the terminal cytoplasm also were observed in the CNGA3$^{-/-}$ retina at 1 month of age. In one case, a free-floating ectopic synaptic ribbon was observed in a bipolar cell dendrite postsynaptic to a cone terminal in a 1-month-old CNGA3$^{-/-}$ retina (Fig. 7G). By 12 months of age, cone terminals were difficult to identify ultrastructurally in the CNGA3$^{-/-}$ retina and often appeared "fragmented." All cone terminals observed in the 12-month-old CNGA3$^{-/-}$ retina showed degraded ultrastructural organization, although synaptic ribbons anchored to the presynaptic membrane and flat contacts could still be found in some cone terminals (Fig. 7H). It should be noted that ultrastructural anomalies associated with cone terminals and their postsynaptic partners also were occasionally observed in the wild-type retina at 12 months of age.

We also examined rod terminals to determine whether the loss of CNGA3 might also affect the synaptic organization of rods (Fig. 8). Rod terminals showing normal synaptic ultrastructure were found in wild-type and CNGA3$^{-/-}$ retina at all ages (Fig. 8A–D), with synaptic complexes organized around a synaptic ribbon anchored to the plasma membrane, abundant synaptic vesicles presynaptically, and the typical triad of postsynaptic processes from horizontal and bipolar cells. However, a variety of ultrastructural aberrations also were observed in rod terminals in the CNGA3$^{-/-}$ retina at 1 and 12 months of age, consistent with decreased rod and rod-driven responses observed in the ERG recordings. Abnormalities observed in

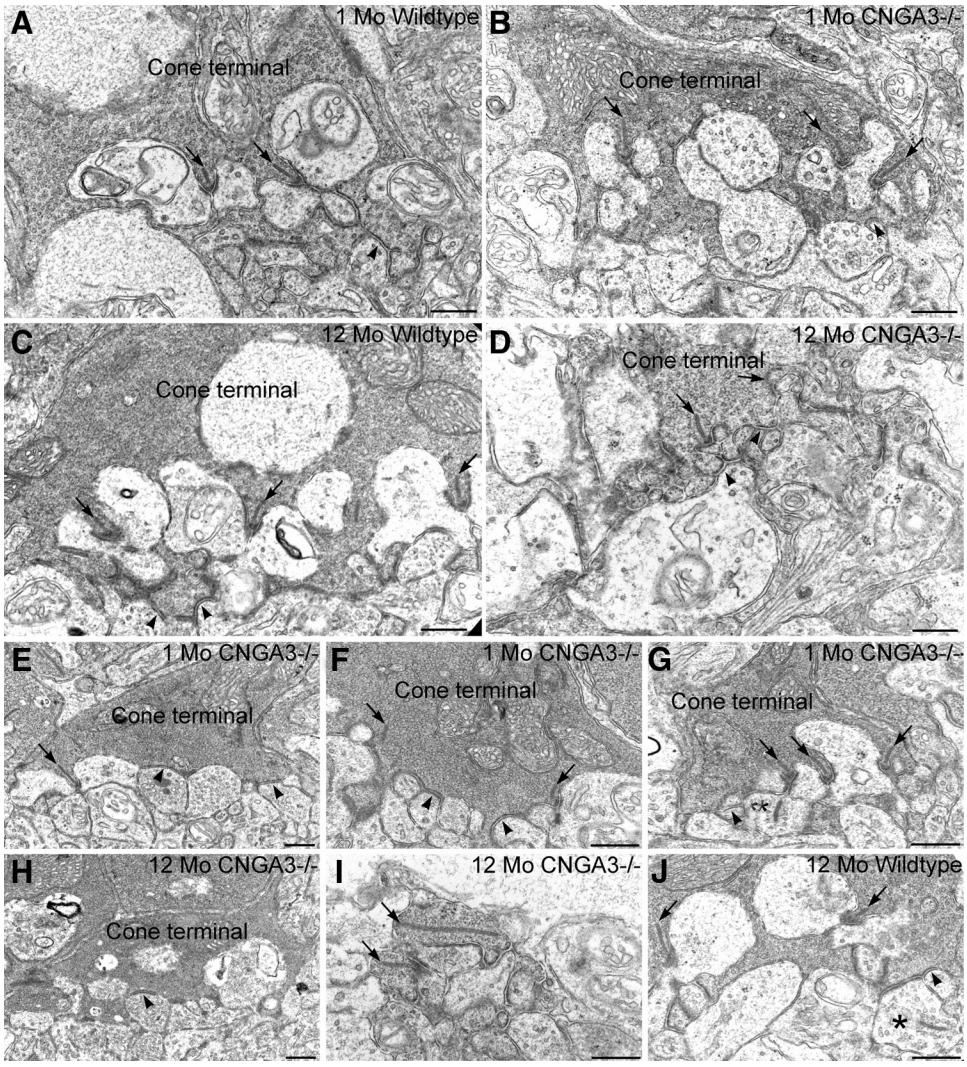

FIGURE 7. Ultrastructural organization of cone synapses is disturbed in the CNGA3$^{-/-}$ retina. Normal synaptic organization in cone terminals of WT (**A**) and CNGA3$^{-/-}$ (**B**) retinas at 1 month of age. Cone terminals have multiple synaptic complexes organized around synaptic ribbons (*arrows*) anchored to the presynaptic plasma membrane with a complex of postsynaptic processes arising from horizontal and bipolar cells. Flat contacts with dendrites from OFF-cone bipolar cells also are present along the base of the cone terminal (*arrowheads*). Synaptic organization in cone terminals of WT (**C**) and CNGA3$^{-/-}$ (**D**) retinas at 12 months of age. Organization of ribbon synaptic complexes (*arrows*) and flat contacts (*arrowheads*) is normal in the WT cone terminal. The ultrastructural organization of synaptic ribbon complexes is degraded in the CNGA3$^{-/-}$ cone terminal, although normal-appearing flat contacts onto the base of the cone terminal are still present. Synaptic anomalies associated with CNGA3$^{-/-}$ cone terminals at 1 month of age; (**E**) cone terminal showing a synaptic ribbon (*arrow*) that contacts an abnormal collection of postsynaptic processes that all show characteristics of horizontal cell processes. Flat contacts can also be seen (*arrowheads*). (**F**) Cone terminal showing free-floating synaptic ribbons (*arrows*). Normal-appearing flat contacts are present (*arrowheads*). (**G**) Cone terminal showing multiple synaptic ribbon complexes (*arrows*). The ribbon at the right contacts only a single postsynaptic process. The bipolar cell dendrite (*) in the ribbon synaptic complex at the left contains an ectopic synaptic ribbon. Normal appearing flat contacts are present (*arrowheads*). Synaptic anomalies associated with CNGA3$^{-/-}$ cone terminals at 12 months of age; (**H**) cone terminal lacking synaptic ribbon complexes. Flat contacts, however, are present (*arrowhead*). (**I**) In the CNGA3$^{-/-}$ retina at 12 months of age, photoreceptor terminals appeared fragmented and could be positively identified only by their electron-dense cytoplasm and the presence of synaptic ribbons (*arrows*). (**J**) Occasional anomalies also were observed in WT cone terminals at 12 months of age. In addition to the expected ribbon synaptic complexes and flat contacts (*arrows* and *arrowheads*, respectively), an ectopic synaptic ribbon (*) is present in a bipolar cell process making flat contacts with the base of the cone terminal. Scale bar, 500 nm for all panels.

these rod terminals included synaptic complexes lacking synaptic ribbons or possessing ribbons that were abnormally small or exhibiting blebs of ribbon material at their tip or free-floating blebs of ribbon material. However, free-floating blebs of ribbon material also were encountered, on occasion, in wild-type rod terminals.

DISCUSSION

This study investigated rod function and survival during the course of cone degeneration resulting from cone CNG channel deficiency in CNGA3$^{-/-}$ mice. We found secondary impairment of rod function and evidence of secondary rod degeneration and loss in CNGA3$^{-/-}$ mice, consistent with the clinical findings that rods degenerate after loss of cone function and cone degeneration in human achromatopsia patients who have defects in the genes encoding the cone CNG channel.[9,10] The scotopic ERG a-wave amplitude was decreased in CNGA3$^{-/-}$ mice at 9 months and older, indicating a reduced light response of rods. An age-dependent reduction of the scotopic ERG b-wave in CNGA3$^{-/-}$ mice occurred as early as one postnatal month. Because cones start to contribute to the scotopic ERG b-wave at light intensities of -0.5 log cd s m^{-2} and higher,[37] we cannot exclude that the reduction in scotopic ERG b-wave observed in younger CNGA3$^{-/-}$ mice is attributable to the loss of cone photoreceptor function. To clarify this we performed ERG recordings to light stimuli of increasing intensities in CNGA3$^{-/-}$ and wild-type mice at 1 month and 12 months. In agreement with a progressive decrease in rod-driven signals, the ERG b-wave amplitude was significantly reduced in 1-month-old CNGA3$^{-/-}$ mice at intensities of -0.03 log cd s m^{-2} or more and in 12-month-old CNGA3$^{-/-}$ mice already at intensities of -0.99 log cd s m^{-2} or more. Hence, the progressive dysfunction and degeneration of cones and their terminals in the OPL of the CNGA3$^{-/-}$ retina leads to changes that compromise rod-driven function before the impairment of rod phototransduction becomes apparent in the scotopic a-wave.

Our ultrastructural studies show that both cones and rods in the CNGA3-deficient retina establish appropriate synaptic con-

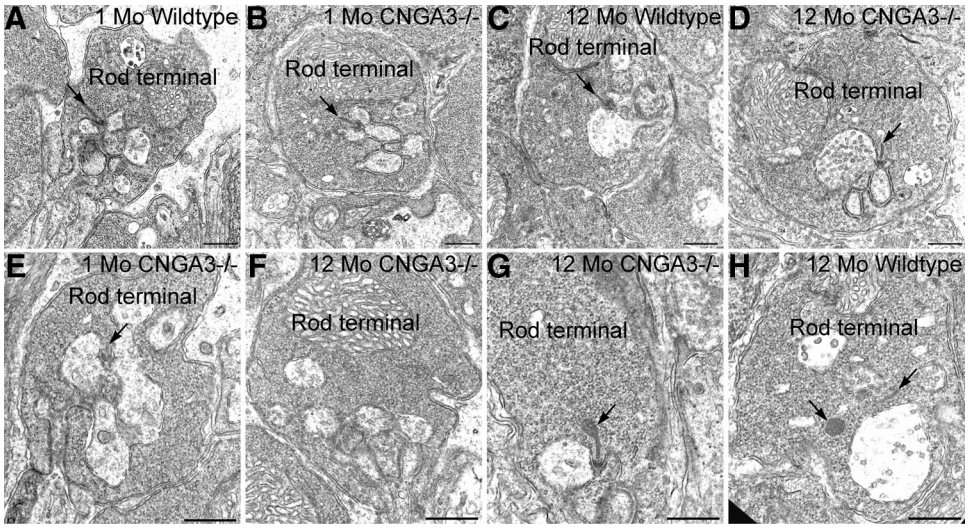

FIGURE 8. The absence of CNGA3 in cones disrupts ultrastructural organization of rod terminals. (**A–D**) Rod terminals in wild-type and CNGA3$^{-/-}$ retinas at 1 and 12 months of age. Wild-type terminals (**A, C**) showed normal synaptic complexes organized around a synaptic ribbon anchored to the presynaptic membrane (*arrows*) and postsynaptic processes from horizontal and bipolar cells. Rod terminals with normal ultrastructure also were present in the CNGA3$^{-/-}$ retina at 1 and 12 months of age (**B, D**). (**E–G**) Rod terminals showing ultrastructural anomalies in the CNGA3$^{-/-}$ retina. (**E**) A rod terminal in the 1-month-old CNGA3$^{-/-}$ retina shows an extremely short synaptic ribbon (*arrow*). (**F**) Rod terminal in the 12-month-old CNGA3$^{-/-}$ retina showing no synaptic ribbon, although postsynaptic processes are present. (**G**) Rod terminal in the 12-month-old CNGA3$^{-/-}$ retina with synaptic ribbon showing bleb of ribbon material at its cytoplasmic tip (*arrow*). (**H**) Wild-type rod terminal at 12 months of age showing a short synaptic ribbon (*arrow*, *right*) and a large, free-floating disc of ribbon material. Scale bar, 500 nm for all panels.

nections initially. Therefore, CNGA3 is not critical to the process of photoreceptor synaptogenesis, which occurs before the onset of light-driven activity in photoreceptors.[38,39] In contrast to the apparent absence of a role for CNGA3 in synaptic development by photoreceptors, the maintenance and function of adult cone photoreceptor synapses depend on the presence of CNGA3, as shown by the gradual loss of the ultrastructural and neurochemical integrity of photoreceptor terminals. Loss of cone terminal integrity was detected as early as one postnatal month. The progressive loss of cone terminals and compromised neurochemical and ultrastructural integrity of surviving cone terminals appears to adversely affect processing of rod signals in the CNGA3$^{-/-}$ retina. One potential mechanism for this change is compromised transmission from rods to rod bipolar cells, which would be consistent with the ultrastructural changes noted in rod terminals in the CNGA3$^{-/-}$ retina. Alternatively, remodeling of inner retinal circuits also might contribute to this impairment, as formation of ectopic cone bipolar cell contacts with rod terminals is known to occur in the CNGA3$^{-/-}$ retina as cone degeneration proceeds.[40] The reduction of the scotopic b-wave before any reduction in the scotopic a-wave suggests that impaired processing of rod signals arises as a result of cone dysfunction and/or loss before any compromise in rod phototransduction. These findings support the idea that the secondary impairment of rod function may first arise at a synaptic level, most likely starting in the OPL. Indeed, synaptic reorganization between photoreceptor terminals and bipolar cell dendrites appears to be a general feature of photoreceptor degeneration,[41,42] and is likely to have profound functional consequences.

The mechanism by which CNGA3 deficiency leads to the gradual degradation of synaptic function and organization in photoreceptor terminals is not obvious. It is unlikely that CNGA3 has a direct role in local regulation of synaptic structure or function, as CNGA3 is localized to COSs and absent from photoreceptor terminals.[43] The progressive loss of synaptic integrity in cone terminals of the CNGA3$^{-/-}$ retina is much more likely to arise from the absence of light-driven activity due to the absence of phototransduction in CNGA3-deficient cones. Photoreceptor synaptic ribbons are known to undergo remodeling of their structure triggered by light onset after a period of darkness, in which the distal end of the synaptic ribbon forms a swelling that then appears to be removed, shortening the ribbon and forming disks of free-floating ribbon material.[44,45] The shortened synaptic ribbons and free-floating ribbon material in photoreceptor terminals in the CNGA3$^{-/-}$ retina closely resemble the appearance of ribbons undergoing normal light-driven remodeling. Normal ribbon remodeling occurs in response to increased illumination and is sensitive to cGMP and Ca^{2+},[44,45] leading to the suggestion that the process is controlled by activation of phototransduction.[45] In the CNGA3$^{-/-}$ retina, however, shortened ribbons, ribbons with distal swellings, and free-floating ribbon material are found in the terminals of cones that do not support phototransduction. This suggests that the processes that normally maintain synaptic ribbons and photoreceptor structure may become dysregulated in the absence of phototransduction, leading to the progressive loss of synaptic integrity observed in the CNGA3$^{-/-}$ retina. Similarly, the light-driven appearance of transient ribbon structures in bipolar cell dendrites has been reported previously in the normal mouse retina.[46] The ribbon structures we observed in bipolar cell dendrites in the CNGA3$^{-/-}$ retina appeared similar to those reported in the normal retina, but appeared adjacent to the terminals of cones that do not produce light responses and, again, may represent a dysregulation of normal, phototransduction-dependent processes. Of note, impaired rod-driven signaling (as shown by a reduced scotopic ERG b-wave) is also observed in cone PDE-deficient mice (cpfl1 mice)[47] and Gnat2-deficient mice (cpfl3 mice).[48] Together, these findings suggest that dysregulation of synaptic maintenance arising from the loss of cone phototransduction may be a shared contributor to secondary rod degeneration in retinal degenerations arising from defects in cone-specific transduction proteins.

We observed evidence indicating the presence of secondary rod degeneration in aged CNGA3$^{-/-}$ mice, as indicated by a progressive reduction in ONL thickness exceeding that predicted by cone loss alone, and reduced expression of rod-specific proteins compared with age-matched wild-type mice. In addition to the loss of photoreceptors from the ONL, the INL and IPL in the CNGA3$^{-/-}$ retina at 9 and 12 months also appeared to be thinned compared with the age-matched wild-type retina, suggesting that CNGA3 deficiency may also lead to secondary loss of cells in the inner retina. Indeed, a similar observation has been reported in cpfl1 mice.[47] Rod degeneration secondary to cone death has been reported in a zebrafish model of cone degeneration resulting from cone PDE deficiency.[49] After cone degeneration in this model, the rods in

retinal regions characterized by low rod density then proceed to degenerate, while rods located in retinal regions characterized by high rod density appear to be protected from degeneration. Therefore, the authors proposed that cell density plays a key role in determining whether rods degenerate as a secondary consequence of cone degeneration.[49] Another potential mechanism underlying the secondary rod degeneration could be aberrant gap junctional coupling of photoreceptors.[50] Rods and cones are anatomically coupled to one another by gap junctions,[51,52] allowing direct passage of signals between rod and cone terminals that can then be transmitted to the inner retina. A recent mathematical modeling study suggested that a direct rod-cone interaction, consistent with gap junctional coupling, is needed for survival of both rods and cones.[53]

The mechanism of cone degeneration secondary to rod degeneration has been intensively studied in human RP patients and in animal models of RP.[1–4] In RP, rod degeneration precedes the secondary degeneration of cones, which eventually leads to complete loss of all photoreceptors and total blindness. Potential mechanisms proposed to underlie secondary cone death include oxidative stress/toxicity, loss of nutritional support, and loss of cell-cell interaction/support.[1–4] Hence, the loss of cone function as RP progresses appears to arise from the loss of the cones themselves. To date it has not been clear whether secondary rod loss after cone degeneration is responsible for diminished rod-driven light responses, or whether compromised rod function leads to secondary rod degeneration. Our work shows that reduced rod-driven function appears before rod loss in CNGA3$^{-/-}$ mice, suggesting that reduced rod function may contribute to rod degeneration. Thus, the pathogenesis of secondary rod degeneration might be quite different from that of secondary cone degeneration. Indeed, how cone degeneration leads to compromised rod function and subsequent rod degeneration remains to be explored.

In summary, this work demonstrates impairment of rod function, structural integrity, and viability secondary to cone dysfunction and degeneration in a mouse model of cone CNG channel deficiency. Hence, the CNGA3$^{-/-}$ mouse is a cone-rod degeneration model. Loss of cone phototransduction leads to compromised integrity of cone photoreceptor terminals, and subsequently compromises the functional and structural integrity of rod terminals and circuits, impairs rod phototransduction, and ultimately results in rod degeneration and cell death.

Acknowledgments

The authors thank Cynthia Harry, Barbara Nagel, and Eileen Parks for providing excellent technical assistance.

References

1. Punzo C, Kornacker K, Cepko CL. Stimulation of the insulin/mTOR pathway delays cone death in a mouse model of retinitis pigmentosa. *Nat Neurosci.* 2009;12:44–52.
2. Komeima K, Usui S, Shen J, Rogers BS, Campochiaro PA. Blockade of neuronal nitric oxide synthase reduces cone cell death in a model of retinitis pigmentosa. *Free Radic Biol Med.* 2008;45:905–912.
3. Cingolani C, Rogers B, Lu L, Kachi S, Shen J, Campochiaro PA. Retinal degeneration from oxidative damage. *Free Radic Biol Med.* 2006;40:660–669.
4. Komeima K, Rogers BS, Lu L, Campochiaro PA. Antioxidants reduce cone cell death in a model of retinitis pigmentosa. *Proc Natl Acad Sci U S A.* 2006;103:11300–11305.
5. Eksandh L, Kohl S, Wissinger B. Clinical features of achromatopsia in Swedish patients with defined genotypes. *Ophthalmic Genet.* 2002;23:109–120.
6. Nishiguchi KM, Sandberg MA, Gorji N, Berson EL, Dryja TP. Cone cGMP-gated channel mutations and clinical findings in patients with achromatopsia, macular degeneration, and other hereditary cone diseases. *Hum Mutat.* 2005;25:248–258.
7. Defoort-Dhellemmes S, Lebrun T, Arndt CF, et al. Congenital achromatopsia: electroretinogram in early diagnosis [in French]. *J Fr Ophtalmol.* 2004;27:143–148.
8. Moskowitz A, Hansen RM, Akula JD, Eklund SE, Fulton AB. Rod and rod-driven function in achromatopsia and blue cone monochromatism. *Invest Ophthalmol Vis Sci.* 2009;50:950–958.
9. Khan NW, Wissinger B, Kohl S, Sieving PA. CNGB3 achromatopsia with progressive loss of residual cone function and impaired rod-mediated function. *Invest Ophthalmol Vis Sci.* 2007;48:3864–3871.
10. Carroll J, Choi SS, Williams DR. In vivo imaging of the photoreceptor mosaic of a rod monochromat. *Vision Res.* 2008;48:2564–2568.
11. Yau KW, Baylor DA. Cyclic GMP-activated conductance of retinal photoreceptor cells. *Annu Rev Neurosci.* 1989;12:289–327.
12. Cook NJ, Molday LL, Reid D, Kaupp UB, Molday RS. The cGMP-gated channel of bovine rod photoreceptors is localized exclusively in the plasma membrane. *J Biol Chem.* 1989;264:6996–6999.
13. Kaupp UB, Niidome T, Tanabe T, et al. Primary structure and functional expression from complementary DNA of the rod photoreceptor cyclic GMP-gated channel. *Nature.* 1989;342:762–766.
14. Arshavsky VY, Lamb TD, Pugh EN Jr. G proteins and phototransduction. *Annu Rev Physiol.* 2002;64:153–187.
15. Picones A, Korenbrot JI. Spontaneous, ligand-independent activity of the cGMP-gated ion channels in cone photoreceptors of fish. *J Physiol.* 1995;485:699–714.
16. Rebrik TI, Korenbrot JI. In intact cone photoreceptors, a Ca2+-dependent, diffusible factor modulates the cGMP-gated ion channels differently than in rods. *J Gen Physiol.* 1998;112:537–548.
17. Bareil C, Hamel CP, Delague V, Arnaud B, Demaille J, Claustres M. Segregation of a mutation in CNGB1 encoding the beta-subunit of the rod cGMP-gated channel in a family with autosomal recessive retinitis pigmentosa. *Hum Genet.* 2001;108:328–334.
18. Dryja TP, Finn JT, Peng YW, McGee TL, Berson EL, Yau KW. Mutations in the gene encoding the alpha subunit of the rod cGMP-gated channel in autosomal recessive retinitis pigmentosa. *Proc Natl Acad Sci U S A.* 1995;92:10177–10181.
19. Wissinger B, Gamer D, Jagle H, et al. CNGA3 mutations in hereditary cone photoreceptor disorders. *Am J Hum Genet.* 2001;69:722–737.
20. Kaupp UB, Seifert R. Cyclic nucleotide-gated ion channels. *Physiol Rev.* 2002;82:769–824.
21. Thiadens AA, Slingerland NW, Roosing S, et al. Genetic etiology and clinical consequences of complete and incomplete achromatopsia. *Ophthalmology.* 2009;116:1984–1989.e1.
22. Johnson S, Michaelides M, Aligianis IA, et al. Achromatopsia caused by novel mutations in both CNGA3 and CNGB3. *J Med Genet.* 2004;41:e20.
23. Kohl S, Baumann B, Broghammer M, et al. Mutations in the CNGB3 gene encoding the beta-subunit of the cone photoreceptor cGMP-gated channel are responsible for achromatopsia (ACHM3) linked to chromosome 8q21. *Hum Mol Genet.* 2000;9:2107–2116.
24. Kohl S, Varsanyi B, Antunes GA, et al. CNGB3 mutations account for 50% of all cases with autosomal recessive achromatopsia. *Eur J Hum Genet.* 2005;13:302–308.
25. Varsanyi B, Somfai GM, Lesch B, Vamos R, Farkas A. Optical coherence tomography of the macula in congenital achromatopsia. *Invest Ophthalmol Vis Sci.* 2007;48:2249–2253.
26. Andersen MK, Christoffersen NL, Sander B, et al. Oligocone trichromacy: clinical and molecular genetic investigations. *Invest Ophthalmol Vis Sci.* 2010;51:89–95.
27. Thiadens AA, Somervuo V, van den Born LI, et al. Progressive loss of cones in achromatopsia. an imaging study using spectral-domain optical coherence tomography. *Invest Ophthalmol Vis Sci.* 2010;51:5952–5957.
28. Biel M, Seeliger M, Pfeifer A, et al. Selective loss of cone function in mice lacking the cyclic nucleotide-gated channel CNG3. *Proc Natl Acad Sci U S A.* 1999;96:7553–7557.

29. Michalakis S, Geiger H, Haverkamp S, Hofmann F, Gerstner A, Biel M. Impaired opsin targeting and cone photoreceptor migration in the retina of mice lacking the cyclic nucleotide-gated channel CNGA3. *Invest Ophthalmol Vis Sci.* 2005;46:1516–1524.
30. Ding XQ, Harry CS, Umino Y, Matveev AV, Fliesler SJ, Barlow RB. Impaired cone function and cone degeneration resulting from CNGB3 deficiency: down-regulation of CNGA3 biosynthesis as a potential mechanism. *Hum Mol Genet.* 2009;18:4770–4780.
31. Ding XQ, Nour M, Ritter LM, Goldberg AF, Fliesler SJ, Naash MI. The R172W mutation in peripherin/rds causes a cone-rod dystrophy in transgenic mice. *Hum Mol Genet.* 2004;13:2075–2087.
32. Peachey NS, Goto Y, al-Ubaidi MR, Naash MI. Properties of the mouse cone-mediated electroretinogram during light adaptation. *Neurosci Lett.* 1993;162:9–11.
33. Mears AJ, Kondo M, Swain PK, et al. Nrl is required for rod photoreceptor development. *Nat Genet.* 2001;29:447–452.
34. Xu J, Morris L, Fliesler SJ, Sherry DM, Ding XQ. Early onset, slow progression of cone photoreceptor dysfunction and degeneration in CNG channel subunit CNGB3 deficiency. *Invest Ophthalmol Vis Sci.* 2011;52:3557–3566.
35. LaVail MM, Unoki K, Yasumura D, Matthes MT, Yancopoulos GD, Steinberg RH. Multiple growth factors, cytokines, and neurotrophins rescue photoreceptors from the damaging effects of constant light. *Proc Natl Acad Sci U S A.* 1992;89:11249–11253.
36. Sherry DM, Murray AR, Kanan Y, et al. Lack of protein-tyrosine sulfation disrupts photoreceptor outer segment morphogenesis, retinal function and retinal anatomy. *Eur J Neurosci.* 2010;32:1461–1472.
37. Tanimoto N, Muehlfriedel RL, Fischer MD, et al. Vision tests in the mouse: Functional phenotyping with electroretinography. *Front Biosci.* 2009;14:2730–2737.
38. Blanks JC, Adinolfi AM, Lolley RN. Synaptogenesis in the photoreceptor terminal of the mouse retina. *J Comp Neurol.* 1974;156:81–93.
39. Olney JW. An electron microscopic study of synapse formation, receptor outer segment development, and other aspects of developing mouse retina. *Invest Ophthalmol.* 1968;7:250–268.
40. Haverkamp S, Michalakis S, Claes E, et al. Synaptic plasticity in CNGA3(-/-) mice: cone bipolar cells react on the missing cone input and form ectopic synapses with rods. *J Neurosci.* 2006;26:5248–5255.
41. Daniele LL, Lillo C, Lyubarsky AL, et al. Cone-like morphological, molecular, and electrophysiological features of the photoreceptors of the Nrl knockout mouse. *Invest Ophthalmol Vis Sci.* 2005;46:2156–2167.
42. Peng YW, Senda T, Hao Y, Matsuno K, Wong F. Ectopic synaptogenesis during retinal degeneration in the royal college of surgeons rat. *Neuroscience.* 2003;119:813–820.
43. Matveev AV, Quiambao AB, Browning Fitzgerald J, Ding XQ. Native cone photoreceptor cyclic nucleotide-gated channel is a heterotetrameric complex comprising both CNGA3 and CNGB3: a study using the cone-dominant retina of Nrl-/- mice. *J Neurochem.* 2008;106:2042–2055.
44. Adly MA, Spiwoks-Becker I, Vollrath L. Ultrastructural changes of photoreceptor synaptic ribbons in relation to time of day and illumination. *Invest Ophthalmol Vis Sci.* 1999;40:2165–2172.
45. Spiwoks-Becker I, Glas M, Lasarzik I, Vollrath L. Mouse photoreceptor synaptic ribbons lose and regain material in response to illumination changes. *Eur J Neurosci.* 2004;19:1559–1571.
46. Spiwoks-Becker I, Lasarzik I, Vollrath L. Transient synaptic ribbons in the mammalian retina at unusual sites. *J Neurocytol.* 2000;29:81–89.
47. Chang B, Grau T, Dangel S, et al. A homologous genetic basis of the murine cpfl1 mutant and human achromatopsia linked to mutations in the PDE6C gene. *Proc Natl Acad Sci U S A.* 2009;106:19581–19586.
48. Chang B, Dacey MS, Hawes NL, et al. Cone photoreceptor function loss-3, a novel mouse model of achromatopsia due to a mutation in Gnat2. *Invest Ophthalmol Vis Sci.* 2006;47:5017–5021.
49. Stearns G, Evangelista M, Fadool JM, Brockerhoff SE. A mutation in the cone-specific pde6 gene causes rapid cone photoreceptor degeneration in zebrafish. *J Neurosci.* 2007;27:13866–13874.
50. Boudard DL, Tanimoto N, Huber G, Beck SC, Seeliger MW, Hicks D. Cone loss is delayed relative to rod loss during induced retinal degeneration in the diurnal cone-rich rodent Arvicanthis ansorgei. *Neuroscience.* 2010;169:1815–1830.
51. Smith RG, Freed MA, Sterling P. Microcircuitry of the dark-adapted cat retina: functional architecture of the rod-cone network. *J Neurosci.* 1986;6:3505–3517.
52. Bloomfield SA, Dacheux RF. Rod vision: pathways and processing in the mammalian retina. *Prog Retin Eye Res.* 2001;20:351–384.
53. Camacho ET, Colon Velez MA, Hernandez DJ, Rodriguez Bernier U, Van Laarhoven J, Wirkus S. A mathematical model for photoreceptor interactions. *J Theor Biol.* 2010;267:638–646.